Earth System Science Data Discussions
Open Access

Ice thickness and subglacial topography of Swedish reference glaciers revealed by radio-echo sounding

Zhuo Wang[1,2], Neil Ross[3], Thomas Frank[4], Jamie Barnett[2,5], Ilaria Santin[6,7], Martin Houssais[1], Johanna Dahlkvist[1], and Nina Kirchner[1,2,8]

[1]Tarfala Research Station, Stockholm University, Stockholm, Sweden
[2]Bolin Centre for Climate Research, Stockholm University, Sweden
[3]School of Geography, Politics and Sociology, Newcastle University, Newcastle upon Tyne, UK
[4]Department of Earth Sciences, Uppsala University, Uppsala, Sweden
[5]Department of Geological Sciences, Stockholm University, Stockholm, Sweden
[6]Department of Civil, Environmental and Geomatic Engineering, ETH Zurich, Zurich, Switzerland
[7]Swiss Federal Institute for Forest, Snow and Landscape Research (WSL), bâtiment ALPOLE, Sion, Switzerland
[8]Department of Physical Geography, Stockholm University, Stockholm, Sweden

Correspondence: Zhuo Wang (zhuo.wang@su.se) and Nina Kirchner (nina.kirchner@su.se)

Abstract. Sweden currently hosts 270 glaciers, four of which belong to the 61 reference glaciers monitored worldwide. Eight Swedish glaciers disappeared during the warm summer of 2024, and under the global warming scenario associated with current climate policies, all four Swedish reference glaciers (Mårmaglaciären, Storglaciären, Rabots glaciär, and Riukojietna) are projected to vanish within this century. Such change will have implications for people, ecosystems, infrastructure, and local me-

5   teorological processes, highlighting the need to better constrain the resultant emerging post-glacial landscapes. During 2024–2025, we conducted radio-echo sounding (RES) surveys on the four Swedish reference glaciers and obtained a total of 40470 ice thickness point measurements. The mean and maximum measured ice thicknesses are 97 and 242 m for Mårmaglaciären, 88 and 225 m for Storglaciären, 85 and 158 m for Rabots glaciär, and 32 and 87 m for Riukojietna. The corresponding mean ice-thickness uncertainties are 12.0, 12.4, 11.4, and 7.5 m, respectively. The RES-measured ice thicknesses were used to pro-

10 duce high-resolution (10 m × 10 m) maps of ice thickness distribution and subglacial topography for each reference glacier, and to calculate their ice volumes as 0.32 (Mårmaglaciären), 0.25 (Storglaciären), 0.23 (Rabots glaciär), and 0.10 km^3 (Riukojietna). The RES data for the four reference glaciers are available at https://doi.org/10.17043/tarfala-marma-res-survey-1, https://doi.org/10.17043/tarfala-storglaciaren-res-survey-1, https://doi.org/10.17043/tarfala-rabot-res-survey-1, and https://doi.org/10.17043/tarfala-rivgojiehkki-res-survey-1 (Wang et al., 2026b, d, a, c). The ice thickness and subglacial topography for the

15 four reference glaciers are available at https://doi.org/10.17043/tarfala-marma-res-2, https://doi.org/10.17043/tarfala-storglaciaren-res-2, https://doi.org/10.17043/tarfala-rabot-res-2, and https://doi.org/10.17043/tarfala-rivgojiehkki-res-2 (Wang et al., 2025a, d, b, c).

1   Introduction

Observations of glacier change over the last century show that glaciers are retreating and losing mass at an accelerating rate globally (Zemp et al., 2015; Hugonnet et al., 2021). Meanwhile, glacier evolution model projections indicate that 49 ± 9 % to

20 83 ± 7 % of the global glacier population could disappear by 2100 (Rounce et al., 2023). Glacier retreat has wider implications for global sea level (Zemp et al., 2015; WCRP Global Sea Level Budget Group, 2018), regional hydrology (Nesje et al., 2008; Pritchard, 2019), natural hazards (Stoffel and Huggel, 2012; Bondesan and Francese, 2023), hydropower potential (Farinotti et al., 2019b), local meteorological processes (Shaw and Pellicciotti, 2025), ecosystems (Johansson et al., 2025), and tourism (Welling et al., 2015). Scandinavian glaciers are projected to disappear entirely at equilibration under the global warming

25 scenario associated with current policies (+2.7°C relative to pre-industrial levels), whereas they will lose 51–93 % of their mass if warming is limited to +1.5°C, as targeted in the Paris Agreement (Zekollari et al., 2025). During 2023–2024, Swedish glaciers lost 13 % of their total area, with eight Swedish glaciers vanishing in an unprecedented year of mass loss. This loss is almost as large as the cumulative area loss over the previous six years (Houssais et al., in prep.). Four Swedish glaciers have been selected by the World Glacier Monitoring Service (WGMS) as reference glaciers in the global monitoring network, which requires

30 over 30 years of ongoing glaciological mass-balance measurements (WGMS, 2025). These glaciers are Mårmaglaciären (local name Moarhmmáglaciären, hereafter MG), Storglaciären (SG), Rabots glaciär (RG), and Riukojietna (local name Rivgojiehkki, hereafter RIV). Under a +2.7°C warming scenario, the four glaciers are projected to be mostly gone by the year 2067, 2087, 2066, and 2085, respectively (Zekollari et al., 2024, 2025).

Knowledge of present-day ice thickness and subglacial topography is fundamental for both regional and global glacier re-

35 search. Ice thickness is required for calculating ice volume (Gillespie et al., 2024), whilst bed geometry is an essential boundary condition for modelling ice dynamics (Wang et al., 2023). Ice thickness and bed topography are also important for improving projections of glacier evolution (Rounce et al., 2023) and to obtain more accurate estimates of glacier lifetimes. Moreover, accurate subglacial topography enables reliable simulations of meltwater routing, providing insights into hydrological changes within glacier catchments during retreat (Ekblom Johansson et al., 2022). Projections of glacier evolution and hydrological

40 changes facilitate future planning for tourism, infrastructure, and indigenous communities.

Glacier ice thickness can be obtained by direct geophysical measurements, numerical modelling, or the integration of these two approaches. Direct observations are typically achieved through ground-based or airborne radio-echo sounding (RES), providing reliable ice thickness (Lindbäck et al., 2018), with uncertainties ranging from a few meters to several tens of meters. However, conducting RES surveys in harsh and generally inaccessible glacial environments is challenging. Practical obstacles

45 such as crevasses, moulins, and steep slopes often limit the spatial coverage of ground-based measurements, and changing glacier surfaces associated with climate warming further complicate fieldwork conditions.

Modelling techniques used for inverting glacier ice thicknesses are based on mathematical descriptions of ice flow dynamics (Linsbauer et al., 2012; Gantayat et al., 2014) and/or physical constraints such as mass conservation (Farinotti et al., 2009; Morlighem et al., 2011). They can estimate ice thickness based on known surface observations, including surface topography,

50 glacier outlines, mass balance (Frank and van Pelt, 2024), and in some cases, surface velocities (Brinkerhoff et al., 2016; Fürst et al., 2017). The integration of observations and ice thickness modelling, i.e., using models to derive glacier-wide ice thickness distributions from discrete observations, is a reliable method for estimating glacier ice thickness when observations are available (Cui et al., 2020; Grab et al., 2021; Gillespie et al., 2024).

Earth System
Science
Data

Open Access

Discussions

55

In our study, dense ground-based RES surveys were conducted on glaciers MG, SG, RG, and RIV to measure ice thicknesses. These observations were integrated with numerical modelling to generate high-resolution interpolated ice thickness datasets for these four glaciers. Bed topography maps for the four glaciers were calculated by subtracting ice thickness from surface elevation. Evaluation of our observation-based ice thickness and previous modelled ice thickness products demonstrates the importance of ground-truth data in deriving accurate ice thickness and bed topography for reference glaciers. Our results improve and extend the current global glacier thickness database, and provide crucial bed topography for future modelling

60 studies of these four glaciers.

2 Study area

MG (67.08° N, 18.68° E), SG (67.90° N, 18.56° E), RG (67.91° N, 18.48° E), and RIV (68.08° N, 18.05° E) are polythermal glaciers located in the wider Kebnekaise area in northern (Arctic) Sweden (Fig. 1a, b). SG has the world's longest detailed continuous glacier mass balance record, extending from 1945 to the present day (Holmlund, 1987; Holmlund et al., 1996a).

65 The mass balances of MG, RG, and RIV have been measured since 1989, 1981, and 1986, respectively, and all records show a generally negative trend (WGMS, 2025; Tarfala Research Station Staff, 2025a, b, c, d). Furthermore, there has been a shrinkage (frontal position and area) of all Swedish glaciers from 2017 to 2023 (Houssais et al., 2025). Between 2021 and 2023, a consistent decline in the area of the four reference glaciers was observed (Houssais et al., 2025, Table A1). The glacier areas in 2024, determined from satellite imagery, are 3.30, 2.89, 3.20, and 2.42 km^2 for MG, SG, RG, and RIV, respectively (Houssais

70 et al., in prep.).

High-resolution ice surface elevations for the four reference glaciers are available from digital elevation models (DEMs), e.g., ArcticDEM (Porter et al., 2022) or Grid2+ (Lantmäteriet, 2019). MG, SG, and RG are all valley glaciers. MG and SG have aspects of 90° (facing east), while RG has an aspect of 270° (facing west). MG's accumulation zone is in the northwestern part of the glacier, and ice surface elevations gradually decline eastward towards the glacier's terminus (Fig. 1c). At SG, ice

75 from the two accumulation areas, in the northwest and southwest of the glacier, merge into a plateau zone in the centre of the glacier before surface elevations decrease again towards the terminus (Fig. 1d). RG has three accumulation areas in the northeast, southeast, and south. Ice surface elevations decrease downslope from these accumulation areas towards the terminus in the west (Fig. 1e). In contrast to the three aforementioned valley glaciers, RIV is a plateau-glacier, with surface elevations gradually declining from the west to the east (Fig. 1f). RIV's subdued surface topography also leads to a mass balance pattern

80 that differs from those of the other three glaciers, i.e., a lower mass balance gradient and a generally negative mass balance across the glacier (WGMS, 2025; Tarfala Research Station Staff, 2025a, b, c, d).

Previous RES surveys were conducted on parts of the reference glaciers to investigate ice thickness and bed topography, the cold surface layer, and englacial hydrology (Table 1). Bed topography maps are available for SG and RG from 1981 (Björnsson, 1981), and for SG from 1993 (Eriksson, 1993; Herzfeld et al., 1993). However, these maps were hand-contoured based on

85 RES data collected before the introduction of GNSS technology, and therefore involve considerable positioning uncertainty. Due to the unavailability of the previous ice-thickness measurements, the Glacier Thickness Database (GlaThiDa) of the
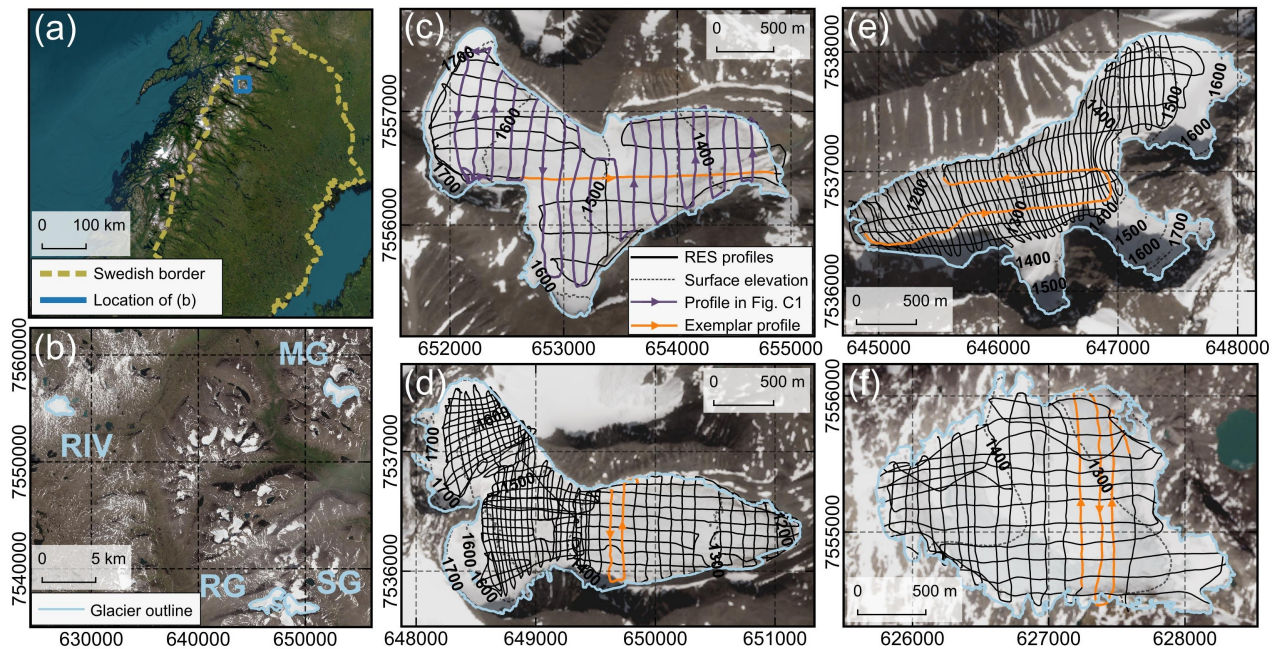
Figure 1. (a) The location of the study area relative to Sweden. The dark blue frame shows the location of Fig. 1b. Background map is from © Esri (Esri, 2025). (b) The locations of four reference glaciers MG, SG, RG, and RIV, in the wider Kebnekaise area. Surface elevation (dashed contours) and RES profiles (solid black lines) for (c) MG, (d) SG, (e) RG, and (f) RIV. The blue lines indicate glacier outlines derived from satellite imagery acquired in 2024-06 (Houssais et al., in prep.). The orange lines represent the exemplar profiles in Fig. 2 as well as Fig. B1–Fig. B3 in Appendix B. The purple line highlights the RES profile shown in Fig. C1. Arrows on the RES profiles indicate the survey directions, corresponding to the radargrams from left to right. The maps (b)–(f) use Sentinel-2 L1C imagery (European Space Agency, 2024) as background. Maps were made in QGIS (QGIS Development Team, 2025).

Global Terrestrial Network does not yet include any point thickness measurements for Swedish reference glaciers (GlaThiDa Consortium, 2020; Welty et al., 2020).

Previous modelled ice thickness for the Swedish reference glaciers (Farinotti et al., 2019a; Millan et al., 2022; Frank and van Pelt, 2024) were based on surface observations, i.e., surface elevation, mass balance, and surface velocity of glaciers, while being predominantly calibrated against bed observations of Norwegian glaciers available in the GlaThiDa. The distance to these bed observations and the climatic differences across Scandinavian mountains have introduced considerable uncertainty in the calibration, and consequently, the estimated ice thickness of Swedish glaciers.

Table 1. Previous RES studies on the four reference glaciers.

Reference	RES survey	Objectives
Björnsson (1981)	1. 1979-03; 1979–04	Map bed topography of SG and RG.
Walford et al. (1986)	2. 1981-09; 1984	Analyse radio-echo records from SG, to estimate bed roughness and distributions of englacial scatters.
Holmlund (1986)	3. 1986-05	Investigate ice thickness based on a 10.1 km RES profile and 10 A-scope pictures on RIV.
Holmlund and Eriksson (1989)	4. 1989-05	Map the cold surface layer on SG.
Herzfeld et al. (1993) and Eriksson (1993)	5. 1989-08; 1990	Map bed topography of SG based on RES surveys 1, 2, 4, and 5.
Holmlund et al. (1996b)	6. 1995-04	Map the longitudinal cold surface layers of SG and MG, and relate them to the climate records.
Glasser et al. (2003)	7. 1997-05	Map the cold surface layer and identify debris layer from the radargram in the terminus of SG.
Pettersson et al. (2003)	8. 1989-04; 2001-04	Map the cold surface layer on SG and investigate the cold surface layer thinning during 1989–2001.
Pettersson et al. (2004)	–	Estimate water content at the cold-temperate transition surface in SG, based on previous RES survey 8.
Pettersson (2005)	–	Investigate frequency dependence of scattering from the cold-temperate transition surface in SG, based on previous RES survey 8.
Jacobel et al. (2001)	9. 2001	Investigate englacial water in the ablation area of SG.
Jacobel et al. (2002)	10. 2002	Investigate englacial water in the ablation area of SG (the second year).
Fountain et al. (2005)	–	Investigate the main pathway of water flow in the ablation area of SG, based on previous RES surveys 9 and 10.
Gusmeroli et al. (2012)	11. 2009	Investigate the cold surface layer thinning on SG during 1989–2009.
Dobiński et al. (2017)	12. 2013-12	Map the longitudinal cold surface layer on SG and relate it to the glacier-permafrost system.
Watts (2024)	13. 2022	Investigate the cold surface layer thinning on SG during 2009–2022.

"–" indicates that no new RES survey was conducted in this study.

Table 2. Survey date, length of RES surveys ("Length"), survey-line spacing ("Spacing") along ("AF") and cross ice flow ("CF"), greatest distance to the nearest known ice-thickness point ("Distance"), and number of RES-measured ice-thickness points after processing ("Points") for MG, SG, RG, and RIV.

Glacier	Survey date	Length (km)	Spacing (m)		Distance (m)	Points
			AF	CF		
MG	2024-04-02	43.6	90–200	70–280	130	6499
SG	2024-03-12; 2024-04-20	82.5	20–210	40–120	150	14360
RG	2025-04-26	65.8	20–90	40–300	210	11544
RIV	2024-03-25	57.6	40–180	90–160	80	8067

3 Methods

3.1 RES data collection

95 RES surveys were conducted on MG, SG, RG, and RIV during 2024–2025, using a Blue System Integration ice penetrating radar (v3), towed behind a snowmobile (Table 2). This portable impulse radar hardware comprises a 1–200 MHz transmitter, digitizer, computer, and a GPS receiver (Mingo and Flowers, 2010). The GPS receiver is a Garmin OEM18x, with a positioning accuracy of 15 m and an update rate of 5 Hz (Garmin International, Inc., 2024). RES data were collected in an in-line antenna

100 configuration, with antenna separation of 15 m, operating at a central wavelength of 16.8 m and a receiver sampling rate of 125 MHz (for MG, SG, RIV) or 250 MHz (for RG). The snowmobile was driven at a steady speed of 4–6 m s^{-1}. The RES signals were stacked 512 times during acquisition, resulting in a trace spacing of 4–6 m during steady driving.

RES surveys were conducted at high spatial density, covering most of each glacier's surface. The greatest distance between any location on each glacier and the nearest known ice-thickness point (RES measurements or glacier outline) is within 210 m.

105 Data acquisition was restricted in the upper accumulation zone of SG (near its western boundary) and in the northeastern upper accumulation zone of RG due to steep surface slope and avalanche risk (Fig. 1d, e). Surveys were not carried out in the southern and southeastern parts of RG because of the rockfall risk. RES profiles were planned along a regular grid, however, field conditions (e.g., crevasses and moulins) resulted in some deviations. The grid spacing varies between 20 and 300 m. The survey trajectory was tracked by the GPS receiver integrated into the RES system. The total length of RES surveys is 249.5 km

110 (Table 2).

3.2 RES data processing and interpretation

The subglacial ice-bed interface, i.e., the glacier bed, is a strong electromagnetic reflector because of the dielectric contrast between ice and bedrock or ice and sediment (Dowdeswell and Evans, 2004). As a result, it appears as a distinct reflection in radargrams. In polythermal glaciers, the cold surface layer has few reflectors or scatterers, making it rela-

115 tively transparent in radargrams. In contrast, water-filled temperate ice is characterised by scattering phenomena and there-
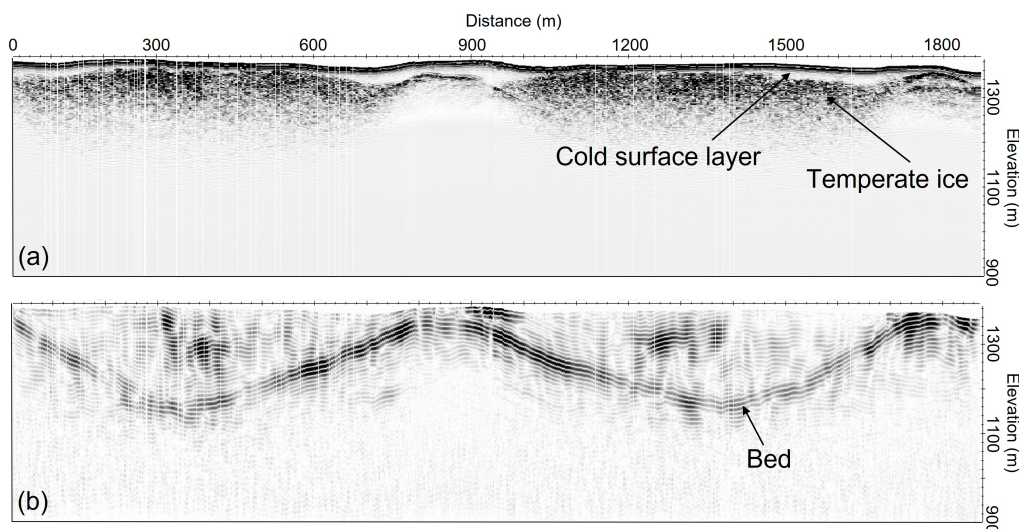
Figure 2. Exemplar RES profile MAR122410H1918 on SG (orange profile in Fig. 1d): (a) RES data after only static correction and topography correction, displaying englacial scattering from temperate ice, and (b) fully processed RES data revealing the glacier bed and the suppression of englacial scattering.

fore appears opaque in radargrams, which can lead to ambiguous bed detection (Schannwell et al., 2014) (Fig. 2a). RES data were post-processed using the ReflexW module for 2-D data analysis (Sandmeier Scientific Software, version 10.5, https://www.sandmeier-geo.de/reflexw.html). The data processing flow, designed to enhance bed reflections, comprises static correction, topography correction, dewow, bandpass filtering, signal gain, and 2-D filtering for valley glaciers MG (Fig. B1),

120 SG (Fig. 2), and RG (Fig. B2). For RIV, which contains relatively shallow ice, a simplified processing flow comprising static correction, topography correction, 2-D filtering, and specifically Kirchhoff migration was applied (Fig. B3). The radargrams have been correctly scaled according to the trace spacing recorded by the GPS.

For polythermal glaciers, the glacier bed is generally picked manually from radargrams (Grab et al., 2021), as strong signal scattering in the temperate ice can complicate automatic or semi-automatic bed identifications (e.g. Fig. 2a). However, manual

125 picking is time-consuming and prone to subjective bias. Therefore, here we combined both automatic and manual approaches for bed identification, to achieve a balance between efficiency, objectivity, and accuracy. The preliminary glacier bed picks, expressed in units of two-way travel time (TWT), were obtained automatically through batch analysis in MATLAB (The MathWorks Inc., 2024) following this workflow: (a) the Hilbert transform was applied to generate an envelope of the processed data; (b) the maximum reflection was identified in each trace and interpreted as the bed; (c) static traces (where GPS trace

130 spacing < 1 m) were removed; (d) adjacent bed picks with large TWT difference were taken as potential erroneous picks and removed; and (e) outlier picks were further filtered using a move median filter, thereby removing surface maximum picks (likely caused by crevasses) as well as other unreliable picks (Fig. C1a). The automatic preliminary bed picks were used to evaluate the data quality and rapidly generate preliminary ice thickness and bed topography maps. The preliminary automatic

Earth System
Open Access Science
Data
Discussions

Table 3. Data statistics for MG, SG, RG, and RIV, including number of crossovers, as well as mean, median, and standard deviation of absolute and relative crossover misfits.

Glacier	Number of crossovers	Absolute misfit (m)			Relative misfit (%)		
		Mean	Median	Std	Mean	Median	Std
MG	334	4.1	3.4	3.2	6.5	4.6	7.7
SG	1864	4.5	3.9	3.3	8.9	5.1	13.7
RG	864	3.8	3.2	3.0	5.9	3.7	7.8
RIV	570	1.9	1.4	1.5	13.2	6.6	18.4

bed picks were then imported into ReflexW for further manual refinement, where misidentified bed picks were repicked. The
135 RES data after static correction only were first used for manual repicking. Fully processed radar data were used as a reference only where the bed reflection was ambiguous or not visible, in order to minimize inaccurate interface tracking caused by filter-induced pulse broadening. In addition, weak bed reflections caused by steeply dipping reflectors or reflectors at great depth, and multiple basal reflectors were unpicked to improve the accuracy of the overall data interpretation (Fig. C1b).

We calculated ice thickness (H) from the TWT of bed picks (t) using a constant radio-wave velocity of 168 m μs^{-1} in ice
140 (v), the same value was used previously for SG (Pettersson et al., 2003) and other glaciers (Dowdeswell and Evans, 2004; Gillespie et al., 2024):

$$H = \frac{tv}{2}. \tag{1}$$

3.3 Uncertainty analysis of RES-measured ice thickness

We assessed the within RES dataset consistency by comparing ice thicknesses at intersection points, i.e., crossovers between
145 survey lines. RES data points from different survey directions less than 5 m apart (the average trace spacing) were considered as crossovers. Ice thicknesses at crossovers exhibit small absolute misfits but larger relative misfit for RIV and near glacier boundaries, primarily affected by the relatively shallow ice in these areas (Table 3). Crossover analysis shows some significant inconsistencies along or near valley walls, and during sharp turns. We accordingly unpicked those bed reflectors to limit the influence of out-of-plane reflections and incomplete extension of the antennas. In total 40470 point values of RES-measured
150 ice thickness were presented for the four reference glaciers (Table 2).

Whilst crossover analysis can reveal inaccurate bed picks by comparing discrepancies between RES measurements, it does not quantify ice-thickness uncertainty for each RES data point. We therefore calculated the uncertainty using standard analytical error propagation methods (Lapazaran et al., 2016). The total uncertainty ϵ_H includes contributions from RES measurement uncertainty $\epsilon_{H_{\text{RES}}}$ and from uncertainty in the positioning of data points $\epsilon_{H_{\text{xy}}}$:

155 $$\epsilon_H = \sqrt{\epsilon_{H_{\text{RES}}}^2 + \epsilon_{H_{\text{xy}}}^2}. \tag{2}$$

Earth System
Science
Data
Open Access
Discussions

Applying error propagation to equation (1), RES measurement uncertainty $\epsilon_{H_{\mathrm{RES}}}$ is a function of radio-wave velocity v, TWT t, their errors ϵ_v and ϵ_t:

$$\epsilon_{H_{\mathrm{RES}}} = \frac{1}{2}\sqrt{v^2\epsilon_t^2 + t^2\epsilon_v^2}. \tag{3}$$

Note that radio-wave velocity v varies spatially, as it is influenced by the density and water/air content of snow, firn, and cold/temperate ice layers. Assuming a constant v for all RES data points (168 m μs^{-1}) can result in biased ice thickness estimates, e.g. overestimations in the ablation zone and underestimations in the accumulation zone. Lapazaran et al. (2016) proposed that uncertainties in v vary from $\sim 1\%$ to $\sim 5\%$, for polythermal glaciers. In our study, we used 5 m μs^{-1} as ϵ_v following Grab et al. (2021). We used range resolution of the RES data as ϵ_t, which represents how precisely the reflections can be identified. Range resolution is generally evaluated between one-quarter and half the RES wavelength, corresponding to 4.2–8.4 m for our unprocessed dataset. Considering the additional uncertainties introduced by data processing and manual interpretation, ϵ_t values of 7 m, 10 m, and 15 m were assigned to bed reflections of varying identification quality.

We estimated the positioning-related ice-thickness uncertainty $\epsilon_{H_{\mathrm{xy}}}$, as the maximum discrepancy in ice thickness between a RES data point and its adjacent points located within ϵ_{xy}, which represents the positioning uncertainty:

$$\epsilon_{\mathrm{xy}} = \sqrt{\epsilon_{\mathrm{xyGPS}}^2 + \epsilon_{\Delta\mathrm{xy}}^2}, \tag{4}$$

ϵ_{xy} has two components, $\epsilon_{\mathrm{xyGPS}}$ is horizontal positioning accuracy of the GPS, and $\epsilon_{\Delta\mathrm{xy}}$ represents the displacement of the RES system occurring within the time lag between the GPS coordinate update and the trace recording (ϵ_T):

$$\epsilon_{\Delta\mathrm{xy}} = v_{\mathrm{RES}}\epsilon_T, \tag{5}$$

where v_{RES} is the travel speed of the RES system, which in our case equals the snowmobile driving speed of 4 m s^{-1}. ϵ_T is estimated as the GPS update period.

3.4 Model-based ice thickness distribution, uncertainty, and bed topography

Due to the ground-based nature of the surveys, RES profiles could not be conducted over areas with moulins, large crevasses, and steep ice surface slopes. We interpolated and extrapolated RES-measured ice thickness to obtain continuous ice thickness distribution (hereafter referred to as "distributed ice thickness" to distinguish them from RES-measured ice thickness) using a model-based approach. Based on Farinotti et al. (2017, 2021) who compared the performance of different ice thickness models, we selected the Glacier Thickness Estimation algorithm (GlaTE) (Langhammer et al., 2019), which performs well where observation data coverage is relatively high. GlaTE is based on mass conservation, apparent mass balances, and Glen's ice flow law. It considers both constraints from RES data and glaciological modelling in inversion.

We input glacier surface elevation, glacier outlines, as well as RES-measured ice thicknesses and their associated uncertainties to GlaTE. ArcticDEM strips acquired closest in time to the RES data acquisition were used as surface elevations. They were acquired in 2022-10-01 (MG), 2024-10-05 (SG), 2024-10-05 (RG), and 2024-05-17 (RIV), respectively, thus ranging from more than 1.5 years before (MG) to a few weeks after (RIV) RES data acquisition in the field. For MG, RG, and RIV,

the ArcticDEM elevations were corrected using vertical offsets of -1.7, 2.5, and -0.1 m based on dGNSS point elevations (Table D1) measured in 2024-04-02 (MG), 2025-04-21 (RG), and 2024-03-25 (RIV), respectively (the dates closest to the RES data acquisition). The -1.7 m adjustment for MG represents cumulative surface elevation changes during the period au-

190   tumn 2022 to spring 2024, whereas the 2.5 m adjustment for RG captures substantial snow accumulation during the winter 2024/2025. The relatively small correction value for RIV is explained by the temporal proximity of the ArcticDEM strip and the RES survey. The ArcticDEM elevation was not corrected for SG because of the lack of dGPS measurements in 2024. Latest glacier outlines identified from 2024 Sentinel-2 imagery (Houssais et al., in prep.) were selected as input for the model, and used to adjust ice thickness at the glacier boundary to zero. RES-measured ice thicknesses and their uncertainties were used to

195   constrain the modelled ice thickness in GlaTE. In the model, we assigned apparent mass balance gradients for the accumulation/ablation zones of MG, SG, RG, and RIV as 0.0056/0.0069, 0.0045/0.0067, 0.0053/0.0063, and 0.00054/0.00098 m w.e. m^{-1} yr^{-1}, respectively, based on mass balance surveys conducted over the most recent three years (WGMS, 2025). We finally obtained distributed ice thickness maps for four reference glaciers with a spatial resolution of 10×10 m. It should be noted that this does not represent the realistic spatial resolution away from the RES survey lines. This is because GlaTE relies on

200   surface information, which physically limits the spatial detail that can be resolved in the modelled bed, i.e. bed features smaller than at least one ice thickness cannot be recovered (Raymond and Gudmundsson, 2005; Gudmundsson and Raymond, 2008).

We repeated the modelling using the maximum and minimum RES-measured ice thickness within the ϵ_H range, the absolute difference between distributed ice thickness was taken as the uncertainty of distributed ice thickness. This estimate represents a lower bound of the true uncertainty, as it does not include uncertainty contributions from the interpolation method and from

205   the surface elevation dataset used. The interpolation uncertainty is related to multiple mechanical and smoothing parameters, while the surface elevation uncertainty depends on data resolution and acquisition time, both of which are difficult to quantify explicitly. The misfit between the distributed ice thickness and RES-measured ice thickness was calculated along RES survey lines.

Bed topography was calculated by subtracting distributed ice thickness datasets from the calibrated surface elevation for

210   each glacier. Our final bed topography products were smoothed using a Gaussian filter with a spatial smoothing scale of approximately 60 m and calibrated to the geoid using geoid model SWEN17_RH2000 (Lantmäteriet, 2017).

4   Data description and evaluation

4.1   RES-measured ice thickness and uncertainty

The RES-measured ice thicknesses were compiled in a similar format as "Table TTT. Glacier thickness: Point measurements" in

215   GlaThiDa (Welty et al., 2020; Gillespie et al., 2024) to ensure the data accessibility and reusability (Wang et al., 2025a, d, b, c). The along track ice thickness data are provided in a CSV (comma-separated values) table containing the following fields: glacier name (GLACIER_NAME), survey date (SURVEY_DATE), RES profile identifier (PROFILE_NAME), RES point identifier (POINT_ID), latitude and longitude of each RES point (POINT_LAT and POINT_LON), calibrated surface elevation (ELE-VATION), ice thickness (THICKNESS), and corresponding ice-thickness uncertainty (UNCERTAINTY).
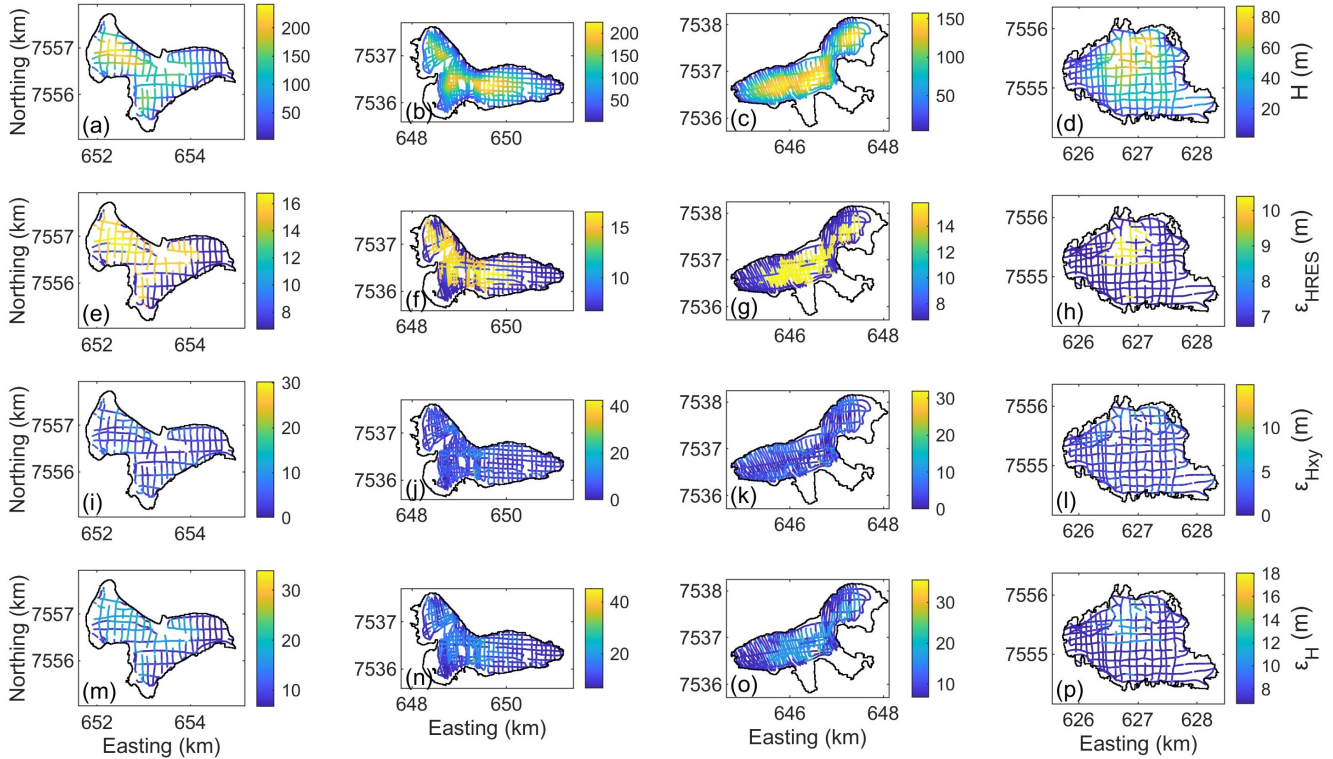
Figure 3. RES-measured ice thickness (a–d), RES measurement uncertainty (e–h), positioning-related ice-thickness uncertainty (i–l), and total ice-thickness uncertainty (m–p) for MG, SG, RG, and RIV (left to right), respectively.

For MG, thickest ice (242 m) is located in the northwestern part. The southern section of the glacier also has relatively thick ice (Fig. 3a). For SG, the thickest ice is found in the central section, where the glacier narrows and then widens into the central plateau region, reaching a maximum of 225 m. In the western accumulation zone there is relatively thick ice of ~200 m (Fig. 3b). For RG, the maximum measured ice-thickness is 158 m in the centre of the glacier after ice converges from the northeastern and southeastern accumulation areas. The northeastern part has relatively thick ice of ~150 m (Fig. 3c). For RIV, the maximum measured ice thickness is 87 m in the northern part of the glacier. Relatively thick ice on RIV is found in its middle-north section (Fig. 3d). Overall, MG is the thickest among the four reference glaciers, followed by SG and RG, while RIV is relatively shallow compared with the other three glaciers (Table 4).

Larger ice-thickness uncertainty related to RES measurement ($\epsilon_{H_{RES}}$) are found where the ice is thicker or the bed is harder to identify in radargrams (Fig. 3e–h). In contrast, ice-thickness uncertainty related to positioning error ($\epsilon_{H_{xy}}$) shows a relatively uniform distribution, with larger values in areas of steeper slopes (Fig. 3i–l). Overall, the total ice-thickness uncertainties (ϵ_H) are primarily related to $\epsilon_{H_{RES}}$ (Fig. 3m–p). Compared with the other three glaciers, RIV has substantially smaller ice thickness and ice-thickness uncertainty (Table 4).

Table 4. Range, mean, and standard deviation of RES-measured ice thicknesses and ice-thickness uncertainties for MG, SG, RG, RIV.

Glacier	H (m)			$\epsilon_{H_{RES}}$ (m)			$\epsilon_{H_{xy}}$ (m)			ϵ_H (m)		
	Range	Mean	Std	Range	Mean	Std	Range	Mean	Std	Range	Mean	Std
MG	2–242	97	58	6.7–16.7	10.7	4.3	0–30.2	4.3	3.5	6.7–33.9	12.0	4.5
SG	2–225	88	54	6.7–16.5	10.3	4.1	0–42.6	5.9	4.4	6.7–45.2	12.4	4.8
RG	4–158	85	42	6.7–15.8	10.0	4.0	0–32.0	4.3	3.3	6.7–35.5	11.4	4.1
RIV	1–87	32	21	6.7–10.4	7.1	1.0	0–14.9	1.9	1.7	6.7–18.0	7.5	1.3

4.2 Distributed ice thickness, uncertainty, and ice volume

Distributed ice thickness maps exhibit the continuous ice thickness variations over each glacier (Fig. 4a, d, g, j). By integrating
235 ice thickness over the glacier area, we obtained ice volume estimates of 0.32 (MG), 0.25 (SG), 0.23 (RG), and 0.10 km^3 (RIV),
respectively.

Consistent with RES observations, MG contains the thickest ice (~240 m) among four reference glaciers (Table 5). MG,
SG, and RG exhibit different ice-thickness patterns. The thickest ice at MG is within its accumulation zone, whereas SG and
RG have the thickest ice in the central sectors, where ice converges from different accumulation areas. The thicker ice at RG
240 extends to the lower ablation area. The differences between the glacier ice thicknesses is likely related to the glacier geometries
(Fig. 1c–d) and bed topography. At RIV, the thickest ice (~80 m) displays a saddle-shaped pattern in the northern sector, which
is consistent with earlier observations Holmlund (1986). The ~20 m difference between our maximum ice thickness and the
previous estimates can be explained by mass loss over the past 28 years.

The uncertainties of distributed ice thickness are relatively large in areas of thick ice, with mean values of 21.7, 20.6, 17.1,
245 and 12.5 m for the four glaciers (Fig. 5a–d). Misfits between distributed ice thickness and RES-measured ice thickness are
larger near the ice margins, where the model assumes zero ice thickness based on the glacier outlines. This occasionally
contradicts the RES measurements, primarily due to temporal asynchrony between the RES surveys and the satellite images
from which the glacier outlines were extracted (Fig. 5e–h).

We compared our distributed ice thickness of four Swedish reference glaciers with those from previous studies (Fig. 4,
250 Table 5). Frank and van Pelt (2024) estimated the ice thickness of Scandinavian glaciers using the Instructed Glacier Model
(Jouvet and Cordonnier, 2023), which is based on a higher-order ice flow approximation. Their approaches (Frank et al., 2023)
incorporated surface elevation (Lantmäteriet, 2019) and its rate of change (Hugonnet et al., 2021), mass balance (Rounce et al.,
2023), and glacier outlines corrected by them from RGI 6.0 (RGI Consortium, 2017) to address systematic misalignment with
topography. Additionally, previous bed elevation for SG (Björnsson, 1981) was used for ice-thickness calibration. The mean
255 absolute ice-thickness misfits between their study and ours are 36, 31, 21, and 73 m for MG, SG, RG, and RIV, respectively
(Fig. 4b, e, h, k). Farinotti et al. (2019a) provided a consensus estimate of global ice thickness using an ensemble of up to five
models considering surface characteristics. Their estimates were based on RGI 6.0 and thus exhibit misaligned glacier outlines
(Fig. 4c, f, i, l). Millan et al. (2022) estimated global ice volumes and ice thicknesses based on high-resolution mapping of
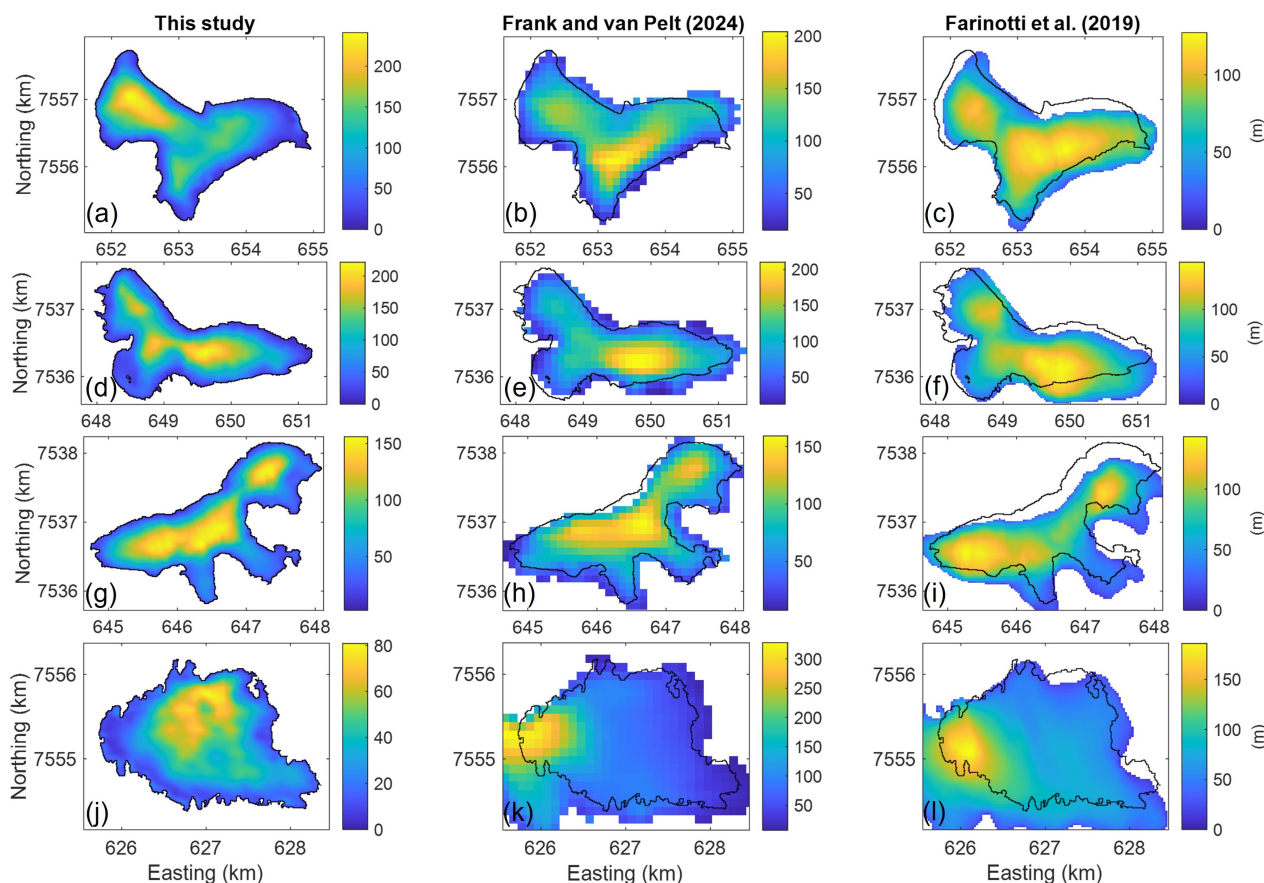
Figure 4. Distributed ice thickness from this study, as well as previous modelled ice thickness from Frank and van Pelt (2024) and Farinotti et al. (2019a) for MG (a–c), SG (d–f), RG (g–i), and RIV (j–l).

ice motion during the period 2017–2018, using glacier outlines from the RGI 6.0. Compared with our results and the other two modelled estimates, these ice thicknesses (Millan et al., 2022) are clearly overestimated, likely related to the model being strongly dependent on the surface flow velocity, which is relatively low (0–18 m yr^{-1} in 2022 reported by Gardner et al. (2024)) and thus difficult to constrain accurately for the four Swedish reference glaciers (Table 5). Therefore, we do not include this study in further comparative analyses.

Previous studies for the four reference glaciers (Frank and van Pelt, 2024; Farinotti et al., 2019a) are based on observational input data obtained in the past, e.g., glacier outlines obtained around 2001–2002 (GLIMS Consortium, 2005). Thus their ice-thickness estimates correspond to an earlier time period than ours. Given the observed ice losses in the recent years, which are quantified as 0.030 (MG), 0.019 (SG), 0.029(RG), and 0.026 km^3 (RIV) during 2017–2024 based on continuous annual mass balance records (Tarfala Research Station Staff, 2025a, b, c, d) and glacier area records (Table A1), the previous studies should show larger ice volumes and ice thicknesses relative to this study. However, Farinotti et al. (2019a) presented smaller mean
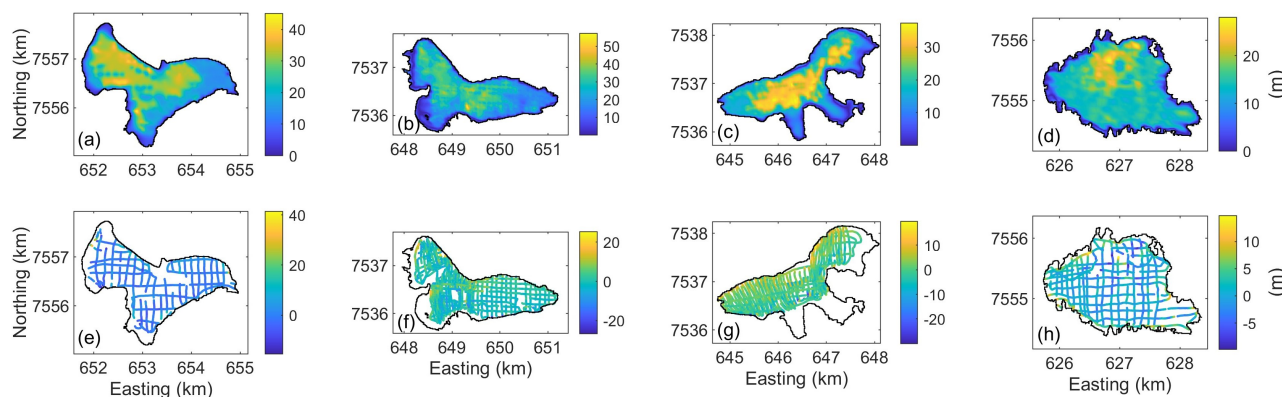
Figure 5. The uncertainty of distributed ice thickness for (a) MG, (b) SG, (c) RG, and (d) RIV. The misfit between distributed ice thickness and RES-measured ice thickness for (e) MG, (f) SG, (g) RG, and (h) RIV.

270   ice thicknesses for MG, SG, and RG, indicating an underestimation of their results. Frank and van Pelt (2024) reported larger ice volumes and mean ice thicknesses for SG, MG, and RG than our study, which are likely related to glacier mass and area losses between their research period and ours. For RIV, both Frank and van Pelt (2024) and Farinotti et al. (2019a) significantly overestimated ice thickness and ice volume as they both relied on the RGI 6.0 glacier outline. This outline corresponds to approximately twice the current RIV area (Fig. 4 j–l), directly affecting the ice volume calculation. Moreover, ice-free terrain

275   included within the overly large outline violates a key requirement for meaningful ice thickness inversions that generally rely on a glacier mask to define the modelling domain, rendering the modelled thicknesses in such areas unreliable.

There are also notable differences in spatial ice-thickness distributions between previous studies and our work (Fig. 4). For MG, our ground-truth RES measurements indicate the thickest ice in the northwest, whereas Frank and van Pelt (2024) and Farinotti et al. (2019a) both reported thicker ice in the south and in the central section while both underestimated ice

280   thickness in the northwestern part (Fig. 4b–c). This underestimation may result from inaccurate mass balance data used in the modelling, but could also arise from assumptions regarding sliding and ice viscosity, surface elevation data input, or incomplete representation of ice flow physics. For SG, both Frank and van Pelt (2024) and Farinotti et al. (2019a) derived the thickest ice in the central glacier (Fig. 4e–f). Similar to our results, Farinotti et al. (2019a) also obtained relatively thick ice in the northwestern part of glacier, while Frank and van Pelt (2024) underestimated the ice thickness there. For RG, Frank and

285   van Pelt (2024) and Farinotti et al. (2019a) showed ice-thickness patterns broadly consistent with our results, i.e. thick ice in the central and northeastern glacier (Fig. 4h–i). Frank and van Pelt (2024) underestimated the ice thickness near to the glacier terminus. For RIV, the ice-thickness distributions from Frank and van Pelt (2024) and Farinotti et al. (2019a) do not agree with our result (Fig. 4k–l), primarily due to inaccurate glacier outlines. Overall, Frank and van Pelt (2024) and Farinotti et al. (2019a) capture the broad patterns of the ice-thickness distribution for MG, SG, and RG. However, Frank and van Pelt (2024)

290   tended to underestimate ice thickness in accumulation zones, whereas Farinotti et al. (2019a) systematically underestimated

Table 5. Comparison of mean distributed ice thicknesses and ice volumes of MG, SG, RG, and RIV obtained in this study and previous studies.

	Glacier	This study	Frank and van Pelt, 2024	Farinotti et al., 2019	Millan et al, 2022
Mean ice thickness (m)	MG	95	97	76	125
	SG	85	89	81	101
	RG	72	76	70	81
	RIV	33	104	74	165
Ice volume (km^3)	MG	0.32	0.37	0.28	0.46
	SG	0.25	0.31	0.28	0.35
	RG	0.23	0.30	0.26	0.30
	RIV	0.10	0.49	0.36	0.80

ice thickness across the glaciers. This comparison highlights the importance of ground-truth RES data for accurately mapping ice-thickness distributions, both for Swedish glaciers and for other glaciers across the world.

4.3 Bed topography

At MG, the subglacial topography reveals a depression in the eastern part of the glacier, with the lowest elevation ~1300 m above sea level (a.s.l., referenced to the geoid model SWEN17_RH2000). The bed gradually rises towards the glacier boundary surrounding this depression, reaching elevations up to ~1800 m a.s.l. along the northwestern and southern margin (Fig. 6a). At SG, an elongated trough is situated in the central-eastern part, containing two depressions at ~1150 m a.s.l.. The bed elevation increases towards the glacier boundary in the southwest, reaching a maximum of ~1700 m a.s.l.. In the northwestern part, there is a depression with an elevation of ~1400 m a.s.l., before the bed rises to ~1900 m.a.s.l. in the uppermost accumulation zone (Fig. 6b). At RG, there is a pronounced deepening along the central section and towards the glacier terminus, where the bed elevation reaches a minimum of ~1100 m a.s.l.. The bed rises towards the three accumulation areas of RG, approaching a maximum elevation of ~1900 m a.s.l. near the southeastern glacier boundary (Fig. 6c). Each of these three glaciers is associated with a trough along its central section, through which ice flows. Distinct from the other three valley glaciers, the glacier bed at RIV does not vary in elevation substantively. Instead, the bed gradually descends from a maximum elevation of ~1430 m a.s.l. in the west to a minimum elevation of ~1200 m a.s.l. in the east (Fig. 6d).

To clearly visualize the topographic variations, we have plotted the bed elevation and surface elevation of selected profiles for four reference glaciers. The small depression in the northwestern section (500–1200 m in Fig. 7a) of MG is associated with thicker ice in the upper glacier, whereas the continuously descending bed in the accumulation zones of SG (Fig. 7b) and RG (Fig. 7c) are associated with the thicker ice in the central and lower parts of these glaciers. The bed descends by only ~120 m along the centreline across RIV, it shows no clear relationship with ice thickness (Fig. 7d).

Our results and previous RES-derived bed topography of SG (Herzfeld et al., 1993; Eriksson, 1993) and RG (Björnsson, 1981) show great consistency in both values and patterns (Fig. 8). Both our and previous maps of SG reveal two depressions
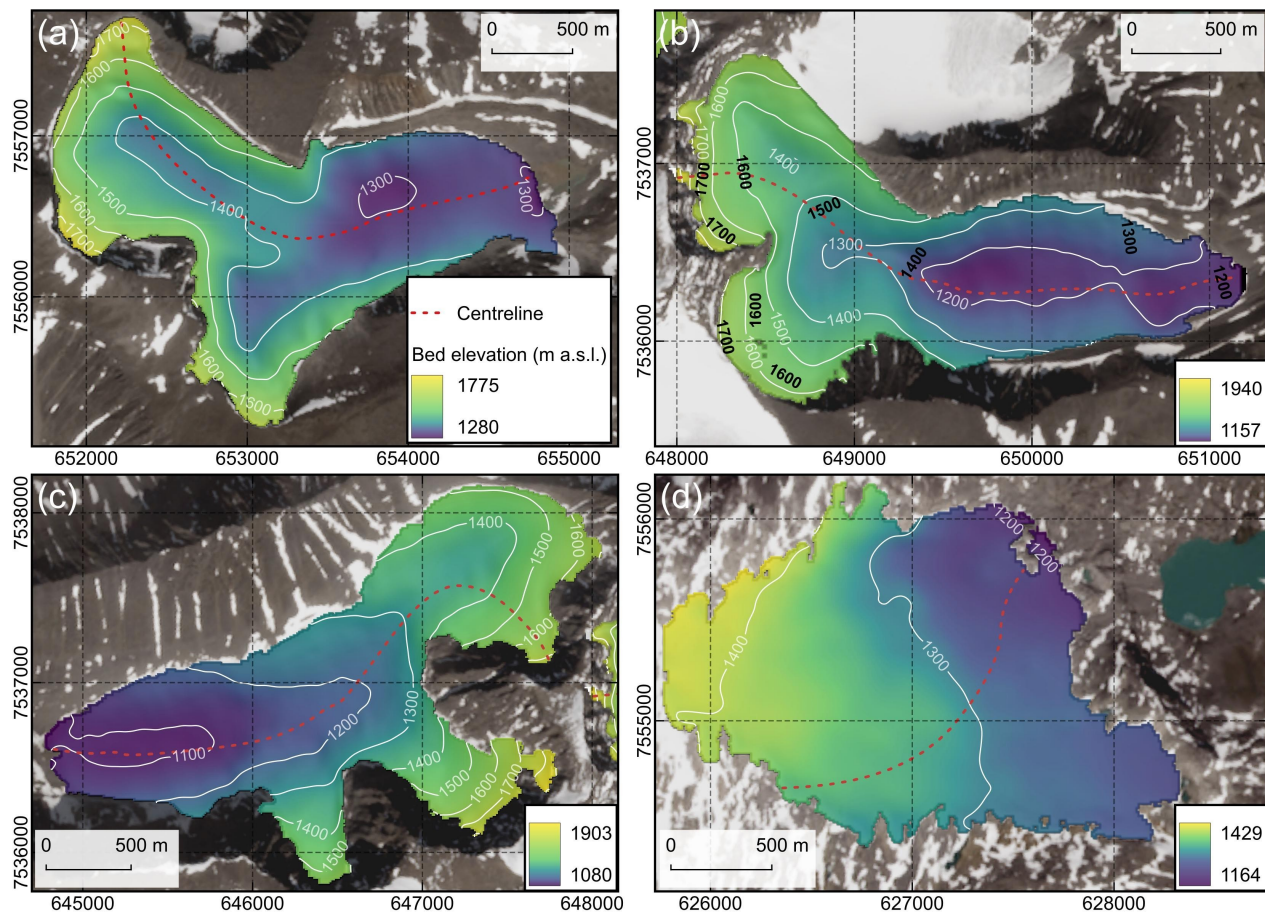
Figure 6. Bed topography of (a) MG, (b) SG, (c) RG, and (d) RIV. White lines represent the contours of bed elevation. Red dashed lines represent the glacier branch centrelines defined in RGI7.0 (RGI Consortium, 2023) and the locations of topographic profiles in Fig. 7. The maps use Sentinel-2 L1C imagery (European Space Agency, 2024) as background.

in the central-eastern section with an elevation of ~1150 m a.s.l., as well as a smaller depression at ~1400–1450 m in the northwestern part. Both maps of RG reveal the deepening along the central section towards the terminus. With denser and more modern RES measurements, our high-resolution maps reveal finer short-wavelength features of topographic variation. Moreover, our digital maps enable reusability in the future.

4.4 Potential applications for the data

Currently, no point measurements of ice thickness from Swedish glaciers are included in the global ice-thickness database GlaThiDa (GlaThiDa Consortium, 2020), our datasets fill this gap and have considerable value across a wide range of disciplines.

Figure 7. The bed elevation (solid line) and surface elevation (dashed line) of selected profiles for (a) MG, (b) SG, (c) RG, and (d) RIV, along their branch centrelines (red lines in Fig. 6). The profiles are oriented from left to right in the direction of decreasing bed elevation.

The ground-truth ice thicknesses can contribute to improving ice-thickness modelling for Swedish glaciers by constraining modelling parameters (such as ice viscosity). For example, we calibrated global model parameters using RES-measured ice thicknesses and repeated the experiment described in Frank and van Pelt (2024) for MG. The model estimates more accurate ice thickness in the northwestern and central section (Fig. E1). The mean absolute misfit between the updated modelled ice thickness and our result is 30 m, representing a 20 % reduction compared with their original modelled misfit.

Our bed topography maps provide essential boundary conditions for numerical modelling. They can be used for future studies of glacier evolution to improve projections of the remaining lifetimes of these glaciers (Zekollari et al., 2025; Rounce et al., 2023). They can also support simulations of future hydrological changes within glacier catchments of four reference glaciers, e.g., determining water routing and locating future glacier lakes (Steffen et al., 2022; Otto et al., 2022).
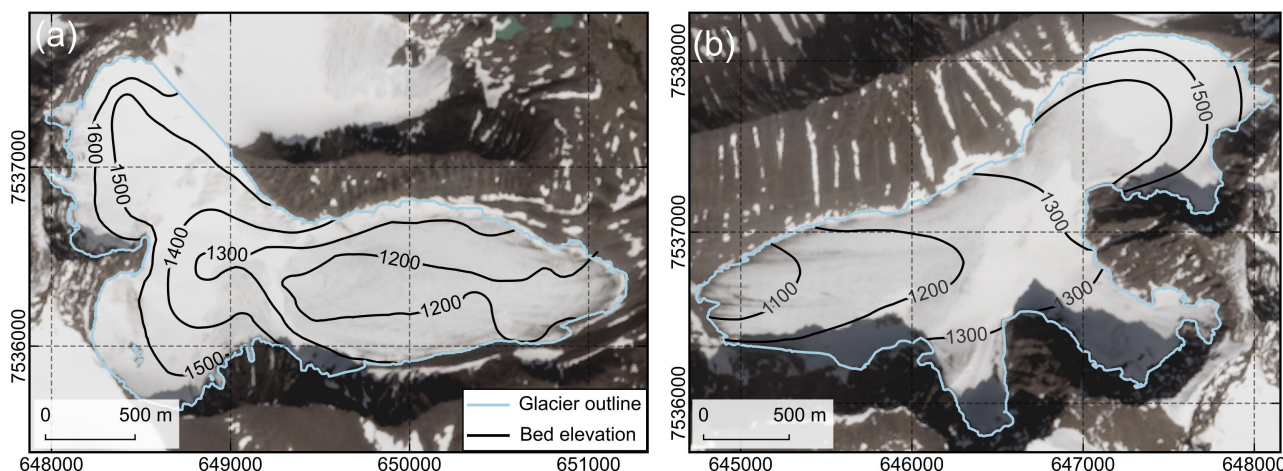
Figure 8. Previous hand-contoured maps of (a) SG bed topography (Herzfeld et al., 1993; Eriksson, 1993) and (b) RG bed topography (Björnsson, 1981). The maps use Sentinel-2 L1C imagery (European Space Agency, 2024) as background. The maps are georeferenced and digitized in QGIS (QGIS Development Team, 2025), with unavoidable errors.

330   Annual ice volumes of the four reference glaciers can be quantified by combining our bed topography maps with annual high-resolution surface DEMs, which can be acquired using uncrewed aerial vehicles. Furthermore, bed topography maps reveal characteristics of the landscapes that will be exposed during the future post-glacial period (Fig. 9). They provide insights into the potential geohazards (e.g. landslides, debris flows, and rockfalls) which might occur as landscape stability changes during glacier retreat.

335   The above predictions are crucial for local policymaking during glacier retreat and in the future post-glacial period, particularly regarding tourism planning, infrastructure development, and sustainable livelihoods of indigenous communities who rely on natural environments for herding.

5   Conclusions

In this study, we compile 40470 ice thickness point measurements collected by RES during 2024–2025 for four Swedish
340   reference glaciers, i.e. MG, SG, RG, and RIV. We observe a mean/maximum ice thickness of 97/242 m, 88/225 m, 85/158 m, and 32/87 m for the four glaciers, respectively, and quantify the measurement uncertainties. Based on these datasets, we produce maps of distributed ice thickness and bed topography with a spatial resolution of 10 m × 10 m. The mean distributed ice thicknesses and ice volumes are 95 m and 0.32 km^3 for SG, 85 m and 0.25 km^3 for MG, 72 m and 0.23 km^3 for RG, and 33 m and 0.10 km^3 for RIV. Our results provide up-to-date ice thickness distribution based on observations. Additionally,
345   we present digital bed topography maps for the four Swedish reference glaciers for the first time. The compiled datasets and derived maps are valuable for future studies on glacier dynamics, and for projecting the evolution of glaciers, landscapes, ecology, and hydrology in the High Arctic mountain environments of northern Scandinavia.
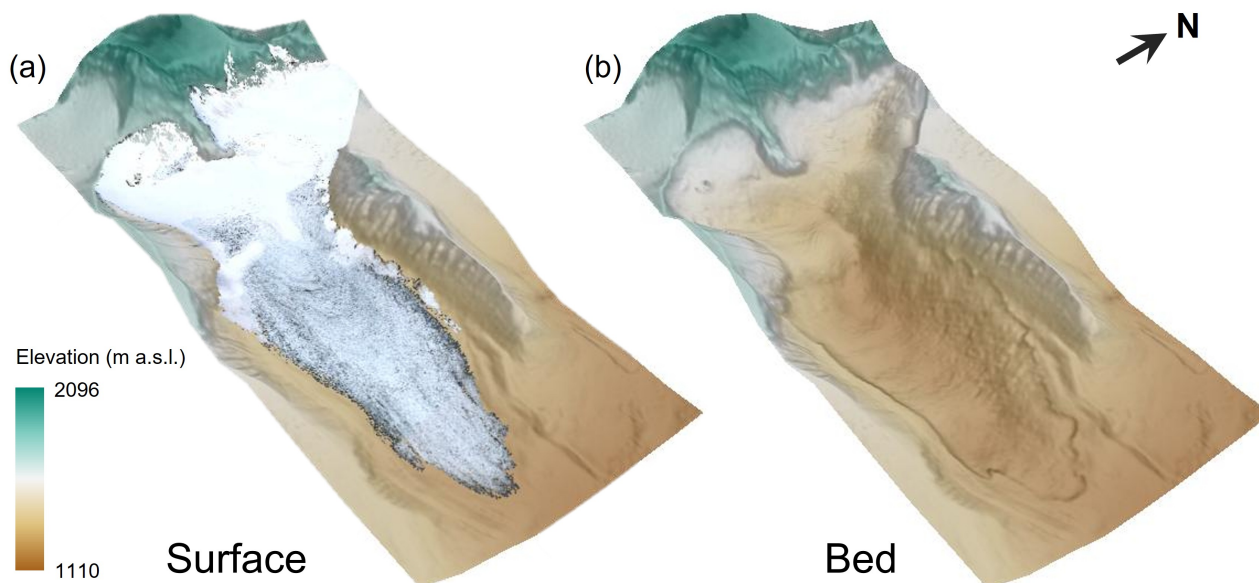
Figure 9. 3D topography of (a) the glacier surface and (b) the bed of SG, illustrating the present-day landscape and the projected post-glacial landscape, respectively.

6 Data availability

The RES data for the four Swedish reference glaciers are available at https://doi.org/10.17043/tarfala-marma-res-survey-1,
350 https://doi.org/10.17043/tarfala-storglaciaren-res-survey-1, https://doi.org/10.17043/tarfala-rabot-res-survey-1, and https://doi.org/10.17043/tarfala-rivgojiehkki-res-survey-1 (Wang et al., 2026b, d, a, c). The compiled datasets of RES-measured ice thicknesses, as well as maps of distributed ice thickness and bed topography for the four Swedish reference glaciers are available at https://doi.org/10.17043/tarfala-marma-res-2, https://doi.org/10.17043/tarfala-storglaciaren-res-2, https://doi.org/10.17043/tarfala-rabot-res-2, and https://doi.org/10.17043/tarfala-rivgojiehkki-res-2 (Wang et al., 2025a, d, b, c).

355 ## 7 Code availability

The code is available at https://zenodo.org/records/18001740 (Wang, 2025).

Appendix A

Table A1. Records of mass balance (Tarfala Research Station Staff, 2025a, b, c, d) and glacier area during period 2017–2024 (Houssais et al., 2025, Houssais et al., in prep.) for MG, SG, RG, and RIV, respectively.

	Year	MG	SG	RG	RIV
Mass balance (m w.e. yr^{-1})	2017	0.26	0.47	-0.18	0.15
	2018	-1.37	-1.60	-1.59	-1.40
	2019	-0.91	-0.31	-0.66	-0.60
	2020	-1.21	0.14	-0.11	-0.70
	2021	-0.76	-0.82	-0.50	-0.82
	2022	-0.43	-0.21	-0.94	-0.80
	2023	-1.26	-0.81	-1.57	-1.35
	2024	-2.57	-2.85	-2.80	-3.46
Glacier area (km^2)	2017	3.52	3.04	3.21	2.97
	2018	3.34	2.95	3.13	2.86
	2019	3.41	2.96	3.17	2.99
	2020	3.48	3.02	3.19	2.96
	2021	3.47	3.02	3.16	2.89
	2022	3.40	2.95	3.14	2.87
	2023	3.34	2.93	3.12	2.81
	2024	3.30	2.89	3.20	2.42

Appendix B

Figure B1. Exemplar RES section (part of profile APRIL2FILE1N) on MG (orange line in Fig. 1c): (a) RES data after static correction and topography correction only, and (b) fully processed RES data revealing the glacier bed.
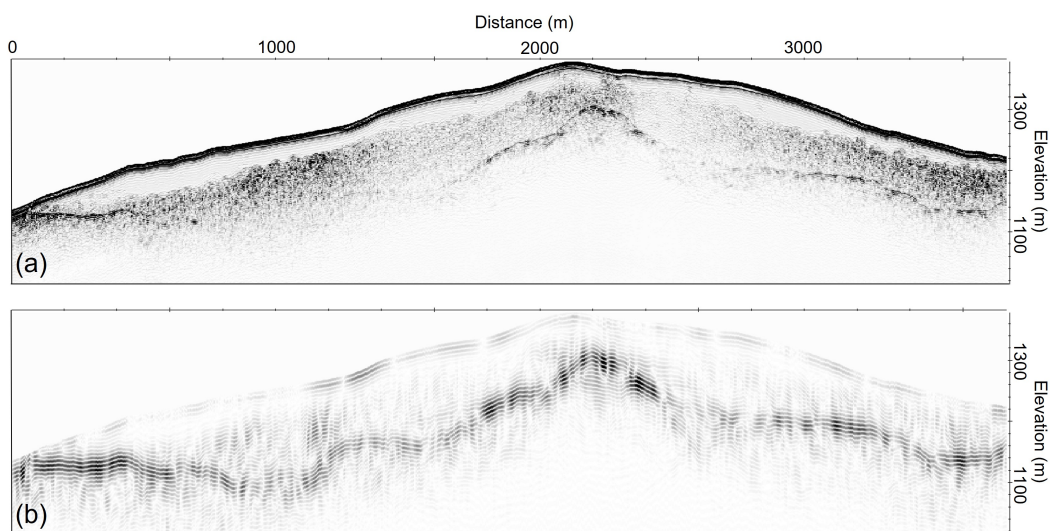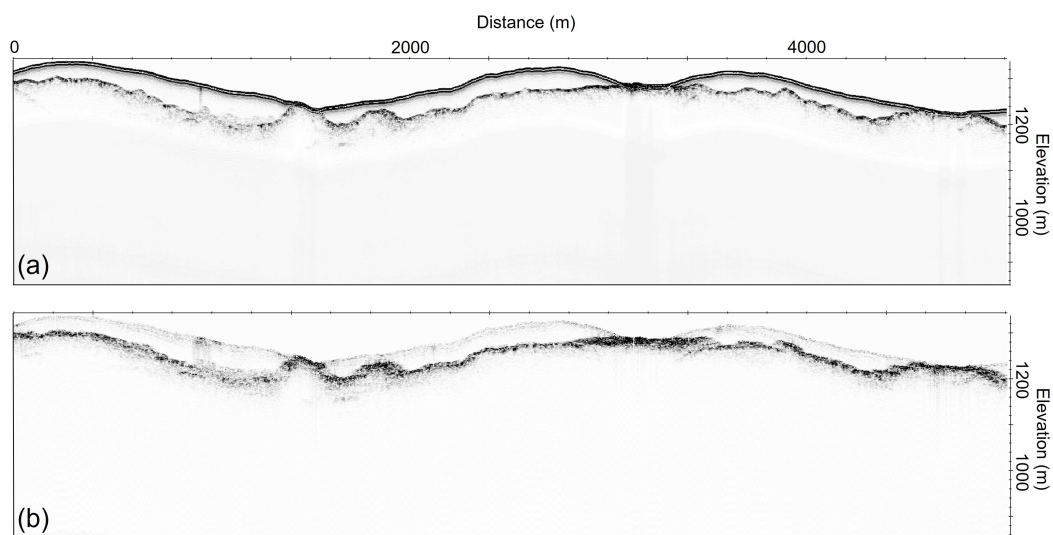
Figure B2. Exemplar RES section (part of profile Apr262511H5602) on RG (orange line in Fig. 1e): (a) RES data after static correction and topography correction only, and (b) fully processed RES data revealing the glacier bed.
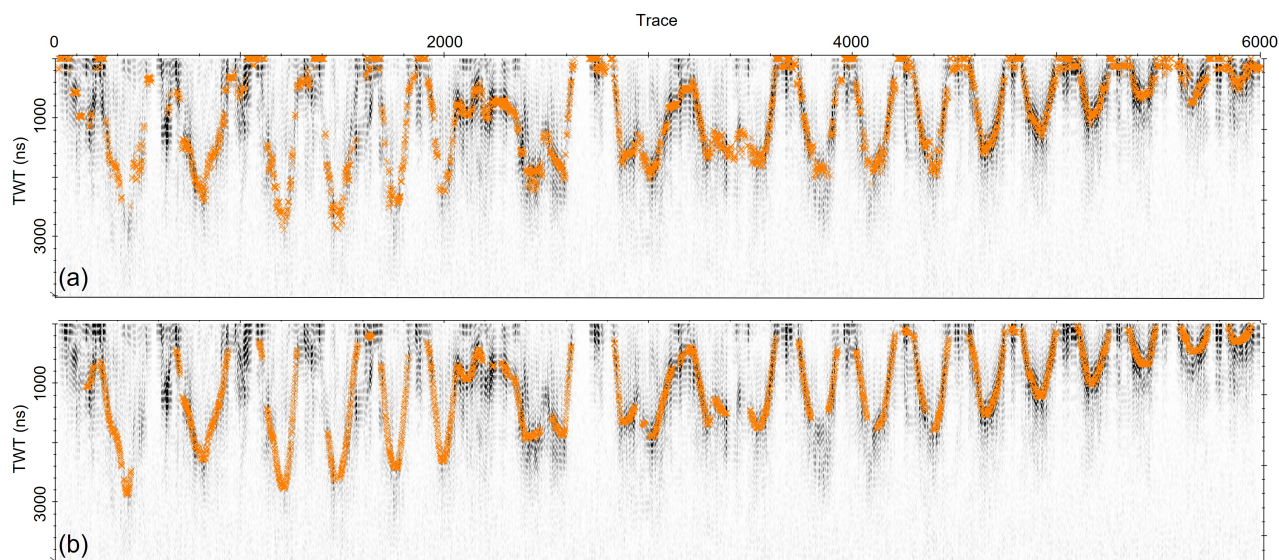
Figure B3. Exemplar RES section (part of profile Mar252411H0212) on RIV (orange line in Fig. 1f): (a) RES data after static correction and topography correction only, and (b) fully processed RES data.

Appendix C

Figure C1. For RES profile APR022414H4605 on MG (the purple profile in Fig. 1c), bed identified (a) automatically in MATLAB, and (b) manually in ReflexW.

360 **Appendix D**

Table D1. Measured dGNSS point elevations for MG, RG, and RIV.

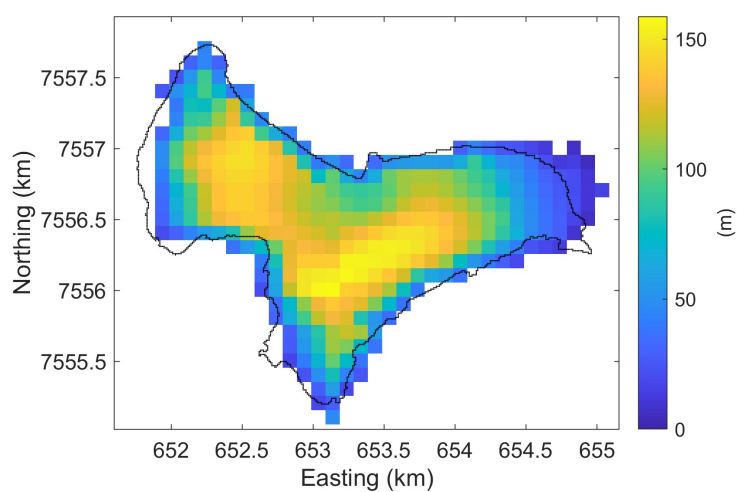| Glacier	Northing (m)	Easting (m)	Elevation (m a.s.l.)	Data acquisition time
MG	7556677.768	652616.782	1583.624	2024-04-02
MG	7557181.258	652113.455	1642.968	2024-04-02
MG	7556425.001	653104.200	1527.505	2024-04-02
MG	7555682.432	653120.809	1523.175	2024-04-02
MG	7556428.683	653856.427	1442.901	2024-04-02
MG	7556671.522	654358.497	1386.505	2024-04-02
RG	7536552.140	645015.787	1162.391	2025-04-21
RG	7536303.458	645489.652	1238.502	2025-04-21
RG	7536804.457	645765.965	1247.427	2025-04-21
RG	7537059.743	645753.849	1233.171	2025-04-21
RG	7537017.581	646279.242	1316.445	2025-04-21
RG	7536368.220	646316.023	1361.250	2025-04-21
RG	7536804.696	646507.402	1335.819	2025-04-21
RG	7536669.133	646800.881	1369.438	2025-04-21
RG	7537556.469	647002.778	1438.607	2025-04-21
RG	7537810.994	647510.627	1505.265	2025-04-21
RIV	7555312.806	626220.099	1419.323	2024-03-25
RIV	7555306.815	626718.847	1404.909	2024-03-25
RIV	7554812.109	626714.732	1387.317	2024-03-25
RIV	7554807.342	627468.122	1331.238	2024-03-25
RIV	7555559.139	627219.108	1313.170	2024-03-25
RIV	7555798.020	627462.592	1251.721	2024-03-25

Appendix E

Figure E1. Updated modelled ice thickness for MG. The experiment follows that of Frank and van Pelt (2024), except that RES-measured ice thicknesses were introduced as constraints for global modelling parameters.

365 *Competing interests.* All authors declare that they have no conflict of interest.

Earth System
Science
Data

Open Access

Discussions

370 **References**

Björnsson, H.: Radio-Echo Sounding Maps of Storglaciären, Isfallsglaciären and Rabots Glaciär, Northern Sweden, Geografiska Annaler: Series A, Physical Geography, 63, 225–231, https://doi.org/10.1080/04353676.1981.11880037, 1981.

Bondesan, A. and Francese, R. G.: The climate-driven disaster of the Marmolada Glacier (Italy), Geomorphology, 431, 108 687, https://doi.org/10.1016/j.geomorph.2023.108687, 2023.

375 Brinkerhoff, D. J., Aschwanden, A., and Truffer, M.: Bayesian Inference of Subglacial Topography Using Mass Conservation, Frontiers in Earth Science, 4, https://doi.org/10.3389/feart.2016.00008, 2016.

Cui, X., Jeofry, H., Greenbaum, J. S., Guo, J., Li, L., Lindzey, L. E., Habbal, F. A., Wei, W., Young, D. A., Ross, N., Morlighem, M., Jong, L. M., Roberts, J. L., Blankenship, D. D., Bo, S., and Siegert, M. J.: Bed topography of Princess Elizabeth Land in East Antarctica, Earth System Science Data, 12, 2765–2774, https://doi.org/10.5194/essd-12-2765-2020, 2020.

380 Dobiński, W., Grabiec, M., and Glazer, M.: Cold–temperate transition surface and permafrost base (CTS-PB) as an environmental axis in glacier–permafrost relationship, based on research carried out on the Storglaciären and its forefield, northern Sweden, Quaternary Research, 88, 551–569, https://doi.org/10.1017/qua.2017.65, 2017.

Dowdeswell, J. A. and Evans, S.: Investigations of the form and flow of ice sheets and glaciers using radio-echo sounding, Reports on Progress in Physics, 67, 1821–1861, https://doi.org/10.1088/0034-4885/67/10/R03, 2004.

385 Ekblom Johansson, F., Bakke, J., Støren, E. N., Gillespie, M. K., and Laumann, T.: Mapping of the Subglacial Topography of Folge-fonna Ice Cap in Western Norway—Consequences for Ice Retreat Patterns and Hydrological Changes, Frontiers in Earth Science, 10, https://doi.org/10.3389/feart.2022.886361, 2022.

Eriksson, M. G.: The Bottom Topography of Storglaciären, Forskningsrapport STOU-NG95, Naturgeografiska Institutionen, Stockholms Universitet, Stockholm, 1993.

390 Esri: World Imagery [basemap], https://www.arcgis.com/home/webmap/viewer.html?useExisting=1&layers= 10df2279f9684e4a9f6a7f08febac2a9, last modified: 24 October 2025, accessed 1 Dec, 2025.

European Space Agency: Sentinel-2 Level-1C imagery, https://browser.dataspace.copernicus.eu/, 2024.

Farinotti, D., Huss, M., Bauder, A., Funk, M., and Truffer, M.: A method to estimate the ice volume and ice-thickness distribution of alpine glaciers, Journal of Glaciology, 55, 422–430, https://doi.org/10.3189/002214309788816759, 2009.

395 Farinotti, D., Brinkerhoff, D. J., Clarke, G. K. C., Fürst, J. J., Frey, H., Gantayat, P., Gillet-Chaulet, F., Girard, C., Huss, M., Leclercq, P. W., Linsbauer, A., Machguth, H., Martin, C., Maussion, F., Morlighem, M., Mosbeux, C., Pandit, A., Portmann, A., Rabatel, A., Ramsankaran, R., Reerink, T. J., Sanchez, O., Stentoft, P. A., Singh Kumari, S., van Pelt, W. J. J., Anderson, B., Benham, T., Binder, D., Dowdeswell, J. A., Fischer, A., Helfricht, K., Kutuzov, S., Lavrentiev, I., McNabb, R., Gudmundsson, G. H., Li, H., and Andreassen, L. M.: How accurate are estimates of glacier ice thickness? Results from ITMIX, the Ice Thickness Models Intercomparison eXperiment,
400 The Cryosphere, 11, 949–970, https://doi.org/10.5194/tc-11-949-2017, 2017.

Farinotti, D., Huss, M., Fürst, J. J., Landmann, J., Machguth, H., Maussion, F., and Pandit, A.: A consensus estimate for the ice thickness distribution of all glaciers on Earth, Nature Geoscience, 12, 168–173, https://doi.org/10.1038/s41561-019-0300-3, 2019a.

Farinotti, D., Round, V., Huss, M., Compagno, L., and Zekollari, H.: Large hydropower and water-storage potential in future glacier-free basins, Nature, 575, 341–344, https://doi.org/10.1038/s41586-019-1740-z, 2019b.

405 Farinotti, D., Brinkerhoff, D. J., Fürst, J. J., Gantayat, P., Gillet-Chaulet, F., Huss, M., Leclercq, P. W., Maurer, H., Morlighem, M., Pandit, A., Rabatel, A., Ramsankaran, R., Reerink, T. J., Robo, E., Rouges, E., Tamre, E., van Pelt, W. J. J., Werder, M. A., Azam, M. F., Li,

H., and Andreassen, L. M.: Results from the Ice Thickness Models Intercomparison eXperiment Phase 2 (ITMIX2), Frontiers in Earth Science, 8, https://doi.org/10.3389/feart.2020.571923, 2021.

Fountain, A. G., Jacobel, R. W., Schlichting, R., and Jansson, P.: Fractures as the main pathways of water flow in temperate glaciers, Nature,
410   433, 618–621, https://doi.org/10.1038/nature03296, 2005.

Frank, T. and van Pelt, W. J. J.: Ice volume and thickness of all Scandinavian glaciers and ice caps, Journal of Glaciology, 70, e11, https://doi.org/10.1017/jog.2024.25, 2024.

Frank, T., van Pelt, W. J., and Kohler, J.: Reconciling ice dynamics and bed topography with a versatile and fast ice thickness inversion, The Cryosphere Discussions, 2023, 1–30, https://doi.org/10.5194/tc-17-4021-2023, 2023.

415   Fürst, J. J., Gillet-Chaulet, F., Benham, T. J., Dowdeswell, J. A., Grabiec, M., Navarro, F., Pettersson, R., Moholdt, G., Nuth, C., Sass, B., Aas, K., Fettweis, X., Lang, C., Seehaus, T., and Braun, M.: Application of a two-step approach for mapping ice thickness to various glacier types on Svalbard, The Cryosphere, 11, 2003–2032, https://doi.org/10.5194/tc-11-2003-2017, 2017.

Gantayat, P., Kulkarni, A. V., and Srinivasan, J.: Estimation of ice thickness using surface velocities and slope: case study at Gangotri Glacier, India, Journal of Glaciology, 60, 277–282, https://doi.org/10.3189/2014JoG13J078, 2014.

420   Gardner, A., Fahnestock, M., Greene, C., Kennedy, J., Liukis, M., Lopez, L., and Scambos, T.: MEASURES ITS_LIVE Regional Glacier and Ice Sheet Surface Velocities, Version 2, https://doi.org/10.5067/JQ6337239C96, 2024.

Garmin International, Inc.: GPS 18x Technical Specifications (Revision B), Olathe, Kansas, USA, https://static.garmin.com/pumac/GPS_18x_Tech_Specs.pdf, 2024.

Gillespie, M. K., Andreassen, L. M., Huss, M., de Villiers, S., Sjursen, K. H., Aasen, J., Bakke, J., Cederström, J. M., Elvehøy, H., Kjøllmoen,
425   B., Loe, E., Meland, M., Melvold, K., Nerhus, S. D., Røthe, T. O., Støren, E. W. N., Øst, K., and Yde, J. C.: Ice thickness and bed topography of Jostedalsbreen ice cap, Norway, Earth System Science Data, 16, 5799–5825, https://doi.org/10.5194/essd-16-5799-2024, 2024.

Glasser, N. F., Hambrey, M. J., Etienne, J. L., Jansson, P., and Pettersson, R.: The Origin and Significance of Debris-charged Ridges at the Surface of Storglaciären, Northern Sweden, Geografiska Annaler: Series A, Physical Geography, 85, 127–147, https://doi.org/10.1111/1468-
430   0459.00194, 2003.

GlaThiDa Consortium: Glacier Thickness Database 3.1.0., https://doi.org/10.5904/wgms-glathida-2020-10, 2020.

GLIMS Consortium: GLIMS Glacier Database, Version 1, https://doi.org/10.7265/N5V98602, 2005.

Grab, M., Mattea, E., Bauder, A., Huss, M., Rabenstein, L., Hodel, E., Linsbauer, A., Langhammer, L., Schmid, L., Church, G., Hellmann, S., Délèze, K., Schaer, P., Lathion, P., Farinotti, D., and Maurer, H.: Ice thickness distribution of all Swiss glaciers based on extended
435   ground-penetrating radar data and glaciological modeling, Journal of Glaciology, 67, 1074–1092, https://doi.org/10.1017/jog.2021.55, 2021.

Gudmundsson, G. H. and Raymond, M.: On the limit to resolution and information on basal properties obtainable from surface data on ice streams, The Cryosphere, 2, 167–178, https://doi.org/10.5194/tc-2-167-2008, 2008.

Gusmeroli, A., Jansson, P., Pettersson, R., and Murray, T.: Twenty years of cold surface layer thinning at Storglaciaren, sub-Arctic Sweden,
440   1989-2009, Journal of Glaciology, 58, 3–10, https://doi.org/10.3189/2012JoG11J018, 2012.

Herzfeld, U. C., Eriksson, M. G., and Holmlund, P.: On the influence of kriging parameters on the cartographic output—A study in mapping subglacial topography, Mathematical Geology, 25, 881–900, https://doi.org/10.1007/BF00891049, 1993.

Holmlund, P.: Radioekosonderingar under 1986, in: Årsrapport från Tarfala forskningsstation 1986, edited by Jansson, P., pp. 50–52, Stockholm University, Department of Physical Geography, Stockholm, Sweden, 1986.

Holmlund, P.: Mass balance of Storglaciären during the 20th century, Geografiska Annaler: Series A, Physical Geography, 69, 439–447, https://doi.org/10.2307/521357, 1987.

Holmlund, P. and Eriksson, M.: The Cold Surface Layer on Storglaciären, Geografiska Annaler: Series A, Physical Geography, 71, 241–244, https://doi.org/10.1080/04353676.1989.11880291, 1989.

Holmlund, P., Karlén, W., and Grudd, H.: Fifty years of mass balance and glacier front observations at the Tarfala Research Station, Geografiska Annaler: Series A, Physical Geography, 78, 105–114, https://doi.org/10.1080/04353676.1996.11880456, 1996a.

Holmlund, P., Näslund, J.-O., and Richardson, C.: Radar Surveys on Scandinavian Glaciers, in Search of Useful Climate Archives, Geografiska Annaler. Series A, Physical Geography, 78, 147–154, https://doi.org/10.2307/520976, 1996b.

Houssais, M., Horemuz, M., Barnett, J., Bergwall, A., and Kirchner, N.: Frontal variations and surface area changes of Swedish glaciers during 2017–2023, Journal of Glaciology, 71, e78, https://doi.org/10.1017/jog.2025.10057, 2025.

Hugonnet, R., McNabb, R., Berthier, E., Menounos, B., Nuth, C., Girod, L., Farinotti, D., Huss, M., Dussaillant, I., Brun, F., and Kääb, A.: Accelerated global glacier mass loss in the early twenty-first century, Nature, 592, 726–731, https://doi.org/10.1038/s41586-021-03436-z, 2021.

Jacobel, R. W., Engle, R. D., Pearson, P. I., and Fountain, A. G.: Radar Investigations of Englacial Water in Storglaciären, Tarfala Research Station Annual Report 1999–2000 and 2000–2001, Tarfala Research Station, 2001.

Jacobel, R. W., Peterson, E. M., Stone, D. R., and Fountain, A. G.: Studies of englacial water in Storglaciären using GPR - year two, Tarfala Research Station Annual Report 2001–2002, Tarfala Research Station, https://www.su.se/polopoly_fs/1.53160.1321256359!/01_02_englacial_water_2.pdf, 2002.

Johansson, E., Islar, M., Shah, M., Gómez-Baggethun, E., Subramanian, S., and Margiotta, C.: Glaciers' contributions to people, nature's values, and coping strategies in the Indian Himalaya, Ecology and Society, 30, https://doi.org/10.5751/ES-16633-300432, 2025.

Jouvet, G. and Cordonnier, G.: Ice-flow model emulator based on physics-informed deep learning, Journal of Glaciology, 69, 1941–1955, https://doi.org/10.1017/jog.2023.73, 2023.

Langhammer, L., Grab, M., Bauder, A., and Maurer, H.: Glacier thickness estimations of alpine glaciers using data and modeling constraints, The Cryosphere, 13, 2189–2202, https://doi.org/10.5194/tc-13-2189-2019, 2019.

Lantmäteriet: SWEN17_RH2000: Sveriges geoidmodell 2017, Tech. rep., Lantmäteriet, https://www.lantmateriet.se/globalassets/geodata/gps-och-geodetisk-matning/presentation-av-swen17_rh2000-j-agren-lang-version-171025.pdf, 2017.

Lantmäteriet: GSD-Elevation data, Grid 2+, https://www.lantmateriet.se/sv/geodata/vara-produkter/produktlista/markhojdmodell-nedladdning/, 2019.

Lapazaran, J. J., Otero, J., Martín-Español, A., and Navarro, F. J.: On the errors involved in ice-thickness estimates I: ground-penetrating radar measurement errors, Journal of Glaciology, 62, 1008–1020, https://doi.org/10.1017/jog.2016.93, 2016.

Lindbäck, K., Kohler, J., Pettersson, R., Nuth, C., Langley, K., Messerli, A., Vallot, D., Matsuoka, K., and Brandt, O.: Subglacial topography, ice thickness, and bathymetry of Kongsfjorden, northwestern Svalbard, Earth System Science Data, 10, 1769–1781, https://doi.org/10.5194/essd-10-1769-2018, 2018.

Linsbauer, A., Paul, F., and Haeberli, W.: Modeling glacier thickness distribution and bed topography over entire mountain ranges with GlabTop: Application of a fast and robust approach, Journal of Geophysical Research: Earth Surface, 117, https://doi.org/10.1029/2011JF002313, 2012.

Millan, R., Mouginot, J., Rabatel, A., and Morlighem, M.: Ice velocity and thickness of the world's glaciers, Nature Geoscience, 15, 124–129, https://doi.org/10.1038/s41561-021-00885-z, 2022.

Mingo, L. and Flowers, G. E.: An integrated lightweight ice-penetrating radar system, Journal of Glaciology, 56, 709–714, https://doi.org/10.3189/002214310793146179, 2010.

485 Morlighem, M., Rignot, E., Seroussi, H., Larour, E., Ben Dhia, H., and Aubry, D.: A mass conservation approach for mapping glacier ice thickness, Geophysical Research Letters, 38, https://doi.org/10.1029/2011GL048659, 2011.

Nesje, A., Bakke, J., Dahl, S. O., Lie, , and Matthews, J. A.: Norwegian mountain glaciers in the past, present and future, Global and Planetary Change, 60, 10–27, https://doi.org/10.1016/j.gloplacha.2006.08.004, 2008.

Otto, J.-C., Helfricht, K., Prasicek, G., Binder, D., and Keuschnig, M.: Testing the performance of ice thickness models to estimate the for-

490 mation of potential future glacial lakes in Austria, Earth Surface Processes and Landforms, 47, 723–741, https://doi.org/10.1002/esp.5266, 2022.

Pettersson, R.: Frequency dependence of scattering from the cold-temperate transition surface in a polythermal glacier, Radio Science, 40, https://doi.org/10.1029/2004RS003090, 2005.

Pettersson, R., Jansson, P., and Holmlund, P.: Cold surface layer thinning on Storglaciären, Sweden, observed by repeated ground penetrating

495 radar surveys, Journal of Geophysical Research: Earth Surface, 108, https://doi.org/10.1029/2003JF000024, 2003.

Pettersson, R., Jansson, P., and Blatter, H.: Spatial variability in water content at the cold-temperate transition surface of the polythermal Storglaciären, Sweden, Journal of Geophysical Research: Earth Surface, 109, https://doi.org/10.1029/2003JF000110, 2004.

Porter, C., Howat, I., Noh, M.-J., Husby, E., Khuvis, S., Danish, E., Tomko, K., Gardiner, J., Negrete, A., Yadav, B., Klassen, J., Kelleher, C., Cloutier, M., Bakker, J., Enos, J., Arnold, G., Bauer, G., and Morin, P.: ArcticDEM - Strips, Version 4.1,

500 https://doi.org/10.7910/DVN/C98DVS, 2022.

Pritchard, H. D.: Asia's shrinking glaciers protect large populations from drought stress, Nature, 569, 649–654, https://doi.org/10.1038/s41586-019-1240-1, 2019.

QGIS Development Team: QGIS Geographic Information System, QGIS Association, https://doi.org/10.5281/zenodo.6139224, 2025.

Raymond, M. J. and Gudmundsson, G. H.: On the relationship between surface and basal properties on glaciers, ice sheets, and ice streams,

505 Journal of Geophysical Research: Solid Earth, 110, https://doi.org/10.1029/2005JB003681, 2005.

RGI Consortium: Randolph Glacier Inventory - A Dataset of Global Glacier Outlines, Version 6, https://doi.org/10.7265/4M1F-GD79, 2017.

RGI Consortium: Randolph Glacier Inventory - A Dataset of Global Glacier Outlines, Version 7, https://doi.org/10.5067/F6JMOVY5NAVZ, 2023.

Rounce, D. R., Hock, R., Maussion, F., Hugonnet, R., Kochtitzky, W., Huss, M., Berthier, E., Brinkerhoff, D., Compagno, L., Copland,

510 L., Farinotti, D., Menounos, B., and McNabb, R. W.: Global glacier change in the 21st century: Every increase in temperature matters, Science, 379, 78–83, https://doi.org/10.1126/science.abo1324, 2023.

Schannwell, C., Murray, T., Kulessa, B., Gusmeroli, A., Saintenoy, A., and Jansson, P.: An automatic approach to delineate the cold–temperate transition surface with ground-penetrating radar on polythermal glaciers, Annals of Glaciology, 55, 89–96, https://doi.org/10.3189/2014AoG67A102, 2014.

515 Shaw, T. E. and Pellicciotti, F.: Mountain glaciers will lose their cooling capacity as they shrink, Nature Climate Change, 15, 1150–1151, https://doi.org/10.1038/s41558-025-02448-1, 2025.

Steffen, T., Huss, M., Estermann, R., Hodel, E., and Farinotti, D.: Volume, evolution, and sedimentation of future glacier lakes in Switzerland over the 21st century, Earth Surface Dynamics, 10, 723–741, https://doi.org/10.5194/esurf-10-723-2022, 2022.

Stoffel, M. and Huggel, C.: Effects of climate change on mass movements in mountain environments, Progress in Physical Geography: Earth

520 and Environment, 36, 421–439, https://doi.org/10.1177/0309133312441010, 2012.

Tarfala Research Station Staff: Glacier surface mass balance for Storglaciären, Northern Sweden, https://doi.org/10.17043/TARFALA-STORGLACIAREN-SURFACE-MASS-BALANCE-1, 2025a.

Tarfala Research Station Staff: Glacier surface mass balance for Moarhmmáglaciären, Northern Sweden, https://doi.org/10.17043/TARFALA-MARMA-SURFACE-MASS-BALANCE-1, 2025b.

525 Tarfala Research Station Staff: Glacier surface mass balance for Rivgojiehkki, Northern Sweden, https://doi.org/10.17043/TARFALA-RIVGOJIEHKKI-SURFACE-MASS-BALANCE-1, 2025c.

Tarfala Research Station Staff: Glacier surface mass balance for Rabots glaciär, Northern Sweden, https://doi.org/10.17043/TARFALA-RABOT-SURFACE-MASS-BALANCE-1, 2025d.

The MathWorks Inc.: MATLAB R2024a, https://www.mathworks.com, 2024.

530 Walford, M. E. R., Kennett, M. I., and Holmlund, P.: Interpretation of Radio Echoes from Storglaciären, Northern Sweden, Journal of Glaciology, 32, 39–49, https://doi.org/10.3189/S0022143000006857, 1986.

Wang, Z.: Code associated with the manuscript "Ice thickness and subglacial topography of Swedish reference glaciers revealed by radio-echo sounding"., https://doi.org/10.5281/zenodo.18001740, 2025.

Wang, Z., Chung, A., Steinhage, D., Parrenin, F., Freitag, J., and Eisen, O.: Mapping age and basal conditions of ice in the Dome Fuji region,
535 Antarctica, by combining radar internal layer stratigraphy and flow modeling, The Cryosphere, 17, 4297–4314, https://doi.org/10.5194/tc-17-4297-2023, 2023, 2023.

Wang, Z., Ross, N., Frank, T., Barnett, J., Santin, I., Houssais, M., Dahlkvist, J., and Kirchner, N.: Ice thickness and bed topography for Moarhmmáglaciären, northern Sweden, https://doi.org/10.17043/tarfala-marma-res-2, 2025a.

Wang, Z., Ross, N., Frank, T., Barnett, J., Santin, I., Houssais, M., Dahlkvist, J., and Kirchner, N.: Ice thickness and bed topography for
540 Rabots glaciär, northern Sweden, https://doi.org/tarfala-rabot-res-2, 2025b.

Wang, Z., Ross, N., Frank, T., Barnett, J., Santin, I., Houssais, M., Dahlkvist, J., and Kirchner, N.: Ice thickness and bed topography for Rivgojiehkki, northern Sweden, https://doi.org/tarfala-rivgojiehkki-res-2, 2025c.

Wang, Z., Ross, N., Frank, T., Barnett, J., Santin, I., Houssais, M., Dahlkvist, J., and Kirchner, N.: Ice thickness and bed topography for Storglaciären, northern Sweden, https://doi.org/10.17043/tarfala-storglaciaren-res-2, 2025d.

545 Wang, Z., Ross, N., Johanna, D., and Kirchner, N.: Raw and processed radio-echo sounding data for Rabots glaciär, northern Sweden, https://doi.org/10.17043/tarfala-rabot-res-survey-1, 2026a.

Wang, Z., Ross, N., and Kirchner, N.: Raw and processed radio-echo sounding data for Moarhmmáglaciären, northern Sweden, https://doi.org/10.17043/tarfala-marma-res-survey-1, 2026b.

Wang, Z., Ross, N., and Kirchner, N.: Raw and processed radio-echo sounding data for Rivgojiehkki, northern Sweden,
550 https://doi.org/10.17043/tarfala-rivgojiehkki-res-survey-1, 2026c.

Wang, Z., Ross, N., and Kirchner, N.: Raw and processed radio-echo sounding data for Storglaciären, northern Sweden, https://doi.org/10.17043/tarfala-storglaciaren-res-survey-1, 2026d.

Watts, H.: Exploring beneath the surface of glacial landscapes: Implementing and improving geophysical investigations in glaciated environments, Ph.D. thesis, Department of Physical Geography, Stockholm University, https://urn.kb.se/resolve?urn=urn:nbn:se:su:diva-224094,
555 2024.

WCRP Global Sea Level Budget Group: Global sea-level budget 1993–present, Earth System Science Data, 10, 1551–1590, https://doi.org/10.5194/essd-10-1551-2018, 2018.

Welling, J. T., Árnason, , and Ólafsdottír, R.: Glacier tourism: a scoping review, Tourism Geographies, 17, 635–662, https://doi.org/10.1080/14616688.2015.1084529, 2015.

560 Welty, E., Zemp, M., Navarro, F., Huss, M., Fürst, J. J., Gärtner-Roer, I., Landmann, J., Machguth, H., Naegeli, K., Andreassen, L. M., Farinotti, D., Li, H., and Contributors, G.: Worldwide version-controlled database of glacier thickness observations, Earth System Science Data, 12, 3039–3055, https://doi.org/10.5194/essd-12-3039-2020, 2020.

WGMS: Fluctuations of Glaciers (FoG) Database, https://doi.org/10.5904/wgms-fog-2025-02b, 2025.

Zekollari, H., Huss, M., Schuster, L., Maussion, F., Rounce, D. R., Aguayo, R., Champollion, N., Compagno, L., Hugonnet, R., Marzeion, B.,
565 et al.: Twenty-first century global glacier evolution under CMIP6 scenarios and the role of glacier-specific observations, The Cryosphere, 18, 5045–5066, https://doi.org/10.5194/tc-18-5045-2024, 2024.

Zekollari, H., Schuster, L., Maussion, F., Hock, R., Marzeion, B., Rounce, D. R., Compagno, L., Fujita, K., Huss, M., James, M., Kraaijenbrink, P. D. A., Lipscomb, W. H., Minallah, S., Oberrauch, M., Van Tricht, L., Champollion, N., Edwards, T., Farinotti, D., Immerzeel, W., Leguy, G., and Sakai, A.: Glacier preservation doubled by limiting warming to 1.5°C versus 2.7°C, Science, 388, 979–983,
570 https://doi.org/10.1126/science.adu4675, 2025.

Zemp, M., Frey, H., Gärtner-Roer, I., Nussbaumer, S. U., Hoelzle, M., Paul, F., Haeberli, W., Denzinger, F., Ahlstrøm, A. P., Anderson, B., Bajracharya, S., Baroni, C., Braun, L. N., Cáceres, B. E., Casassa, G., Cobos, G., Dávila, L. R., Granados, H. D., Demuth, M. N., Espizua, L., Fischer, A., Fujita, K., Gadek, B., Ghazanfar, A., Hagen, J. O., Holmlund, P., Karimi, N., Li, Z., Pelto, M., Pitte, P., Popovnin, V. V., Portocarrero, C. A., Prinz, R., Sangewar, C. V., Severskiy, I., Sigurđsson, O., Soruco, A., Usubaliev, R., and Vincent, C.: Historically un-
575 precedented global glacier decline in the early 21st century, Journal of Glaciology, 61, 745–762, https://doi.org/10.3189/2015JoG15J017, 2015.